The field of view of a scintillator pair for cosmic rays

N.G. Schultheiss[*†]

Abstract

Particles in an extended air shower (EAS), initiated by a cosmic ray primary, lead to two nearly simultaneous detections in a scintillator pair. The angle of the EAS and the axis through both scintillators can be reconstructed using the time difference of the detections and the distance between the scintillators. The acceptances of a scintillator along the axis through the scintillators and perpendicularly on this axis follow the same distribution in theory. Using a data set with two perpendicular detector pairs this theory is verified. The distribution of possible origins of cosmic ray primaries, and the resulting EAS, can thus be described using the perpendicular distribution for a given time difference.

Keywords: Cosmic rays, acceptance, HiSPARC

1 Introduction

Cosmic ray primaries initiate extended air showers (EAS) in the atmosphere. The number of secondary particles in an EAS depends both on the energy and the type of the cosmic ray primary particle (foton, electron, proton, nucleus). Along the path in the atmosphere the energy in the EAS is distributed over a growing number of particles. With sufficient energy of the primary particle ($E_p > 10^{14}$ eV) a cascade of secondary particles can reach scintillators on the Earth's surface and are detected. Comparing the zenith angles of cosmic ray primaries with equal energy, an increasing zenith angle leads to an increasing path length for the resulting EAS in the atmosphere. As a result the number of detectable particles that reach the surface will decrease.

In HiSPARC the direction of a cosmic ray primary penetrating the Earth's atmosphere is reconstructed using measurements of EAS particles in scintillators.

*Nikhef
†Zaanlands Lyceum

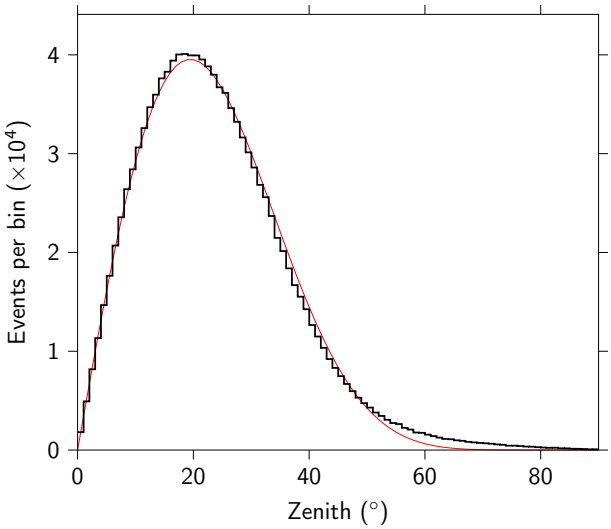

Fig. 1.1: *The measured number of particles as function of the zenith angle θ for Science Park Amsterdam shown as a step histogram. The fitted distribution with $a = 7$ is plotted as a red curve. Diagram from* [1]

This is simulated for a single detector using 10^6 primary particles having random distributions for the zenith angle θ and the azimuth φ. The distribution of $dN(\varphi)/d\varphi$ is flat, because of the symmetry properties around the zenith. The distribution $dN(\theta)/d\theta$ is described as [2, p. 78]:

$$\frac{dN(\theta)}{d\theta} \propto 2\pi \sin(\theta) \cos^a(\theta) \tag{1.1}$$

This distribution has a geometrical and a physical component. The geometrical component can be written as $2\pi \sin(\theta) \cos(\theta)$. The factor $2\pi \sin(\theta)$ is proportional to the celestial area and $\cos(\theta)$ is proportional to the effective area of the detector perpendicular to the displacement of the EAS. The physical component due to the extinction in the atmosphere is described as being proportional to $\cos^{(a-1)}(\theta)$.

The location in space of the detector is time dependent as a result of the rotation of the Earth. This rotation of the Earth is neglected in the simulation shown in fig. 1.2[1]. The majority of the detected particles is caused by the abundant cosmic ray primaries in the range of 10^{14} eV. The distribution of directions of arrival for cosmic rays with this energy is very uniform [2, p. 124-125]. In this case the acceptance is considered independent on the azimuth.

[1] The corresponding atmospheric layer converts a cosmic primary in an EAS and is regarded as a part of the detection setup.

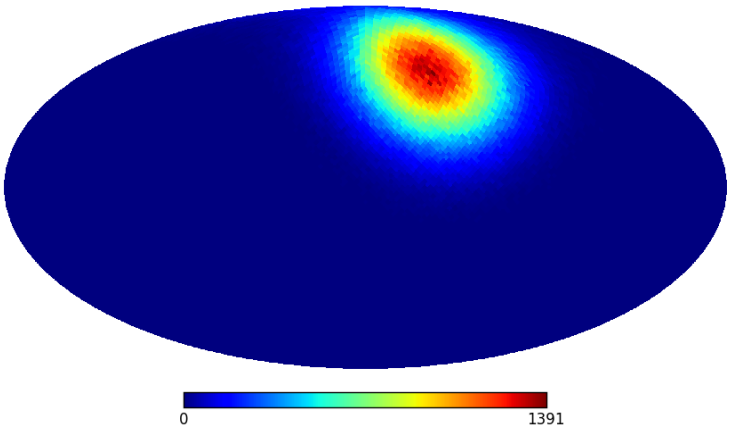

Fig. 1.2: *A simultion of* 10^6 *EAS shown in a Mollweide view (equal area bins) neglecting the Earth's rotation. The number of EAS per unit of area is shown in an equatorial projection. The north or Polaris is in the highest point, south is the lowest point. The zenith of the scintillator is at the center of the colored area.*

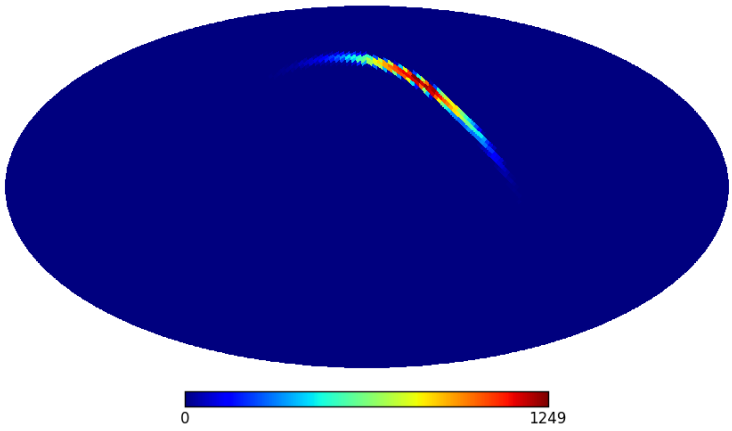

Fig. 1.3: *The dataset of fig. 1.2 is used for the simulation of a station with two detectors. The line connecting the centers of the two scintillators makes an angle of* 45° *with respect to the local meridian. The time difference between detections is* 5ns *with a bin width of* 2.5ns. *The distance between the scintillators is* 10m.

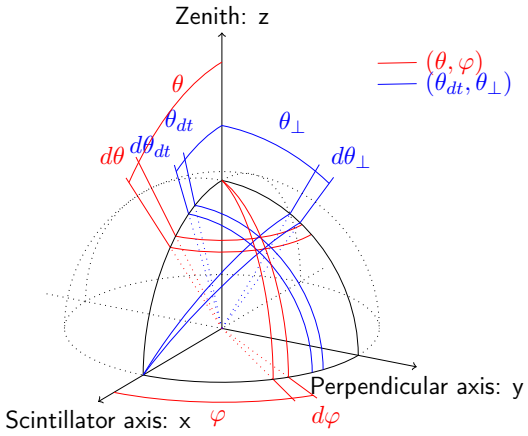

Fig. 2.1: *Two intersecting area's with the same location are described using two polar coordinate systems. The (θ, φ) coordinate system is symmetric around the zenith (shown in red). The $((\pi/2 - \theta_{dt}), \theta_\perp)$ coordinate system is symmetric around the axis through the scintillators (shown in blue).*

Discrimination between background radiation and EAS particles is not possible using a single scintillator. A cosmic ray event is generated when both scintillators detect particles. In this case the EAS spreads particles over an area covering both scintillators. Background radiation only generates a detection in a single scintillator.

An added advantage of a setup using a scintillator pair is the possibility to partially reconstruct the direction of the shower axis (fig. 1.3). The particles in an EAS travel at speeds approximating the speed of light c. The time difference $t_{1,2}$ of the particle detections and the distance d between the scintillators define the angle θ_{dt} of that EAS:

$$\sin(\theta_{dt}) = \frac{c\, t_{1,2}}{d} \tag{1.2}$$

2 Theory

2.1 Distributions

In fig. 2.1 the direction of an EAS is shown as the intersection of a slice and a wedge on a celestial sphere. This intersection usually is expressed in the (θ, φ) or zenith, azimuth polar coordinate system. The sky is symmetric around the axis defined by the zenith. This symmetry leads to equal distributions in slices trough the zenith.

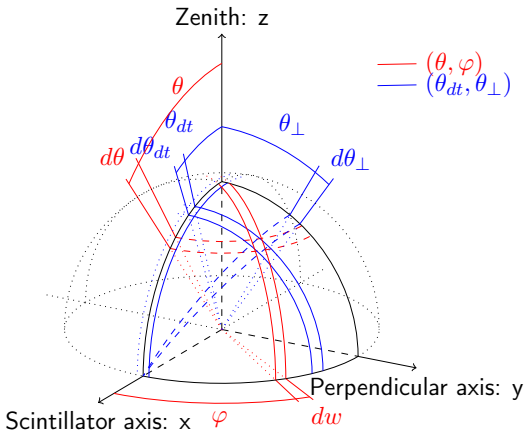

Fig. 2.2: *An area described using the intersections of slices of equal width. The defined area can be reached in two separate ways. Along the red slice the flux can be calculated immediately using θ. The same location is reached in two steps along the blue slices. Along the blue slice trough the scintillator axis the perpendicular slice is reached. The flux is calculated at θ_{dt}, defining the number of particles in the perpendicular slice. The flux of this second set of particles is distributed along the perpendicular slice as a function of $\theta_\perp$ in a similar way.*

The axis through both scintillators defines a symmetry in a detection station. Here a $((\pi/2-\theta_{dt}),\theta_{\perp})$ polar coordinate system is used[2]. The angle θ_{dt} is reconstructed using the time difference in the detections (eq. 1.2). Because of the symmetry, $\theta_{\perp}$ is not directly determinable.

Using eq. 1.1 the number of EAS coming from a circular band (slice) with length $2\pi\sin(\theta)$ and width $d\theta$ can be calculated. In figure 2.1 a segment of the wedge of the celestial half sphere defined by φ and $\varphi+d\varphi$ intersects with a slice defined by θ and $d\theta$ is shown in red. The EAS-flux in the intersecting area is formulated as:

$$\frac{d^2N(\theta,\varphi)}{d\theta d\varphi} \propto \sin(\theta)\cos^a(\theta) \tag{2.1}$$

The width of the wedge is expressed as $\sin(\theta)\,d\varphi$. The equal width dw of a slice, as shown in figure 2.2, is not dependent on θ. This leads to a flux of:

$$\frac{d^2N(\theta,\varphi)}{d\theta dw} \propto \cos^a(\theta) \tag{2.2}$$

Eq. 2.2 is a valid expression for all slices with constant width and through the zenith due to the symmetry around the zenith axis.

The location of an intersection on a unit sphere can be written in the (θ,φ)-frame as:

$$\begin{pmatrix} x \\ y \\ z \end{pmatrix} = \begin{pmatrix} \sin(\theta)\cos(\varphi) \\ \sin(\theta)\sin(\varphi) \\ \cos(\theta) \end{pmatrix} \tag{2.3}$$

And in the $(\theta_{dt},\theta_{\perp})$-frame as:

$$\begin{pmatrix} x \\ y \\ z \end{pmatrix} = \begin{pmatrix} \cos(\pi/2-\theta_{dt}) \\ \sin(\pi/2-\theta_{dt})\sin(\theta_{\perp}) \\ \sin(\pi/2-\theta_{dt})\cos(\theta_{\perp}) \end{pmatrix} = \begin{pmatrix} \sin(\theta_{dt}) \\ \cos(\theta_{dt})\sin(\theta_{\perp}) \\ \cos(\theta_{dt})\cos(\theta_{\perp}) \end{pmatrix} \tag{2.4}$$

The z-coordinate expresses θ as a function of θ_{dt} and $\theta_{\perp}$:

$$z = \cos(\theta) = \cos(\theta_{dt})\cos(\theta_{\perp}) \tag{2.5}$$

Substition of eq. 2.5 in eq. 2.2 leads to:

$$\frac{d^2N(\theta,\varphi)}{d\theta dw} \propto \cos^a(\theta_{dt})\cos^a(\theta_{\perp}) \tag{2.6}$$

Leading to:

[2] It must be noted that the atmospheric depth is dependent on θ_{dt} and $\theta_{\perp}$, this effects the number of particles in the EAS.

$$\frac{d^2N(\theta,\varphi)}{d\theta dw} \propto \frac{d^2N(\theta_{dt},w)}{d\theta_{dt}dw} \times \frac{d^2N(\theta_{\perp},w)}{d\theta_{\perp}dw} \tag{2.7}$$

The mathematical analysis proofs that all distributions in the slices in fig. 2.2 follow the same function.

3 Verification

Stations 501 and 510 both contain four scintillators located on perpendicular axes as shown in fig. 3.1. Each scintillator is equipped with a Photo Multiplier Tube (PMT). Two PMT's are connected via cables to a single HiSPARC electronics unit. A master and a slave unit register all events from two scintillator pairs in one station with a sample frequency of 400MHz with a constant delay for each scintillator. The generated timing errors, due to these constant delays, must be compensated in the algorith.

The resulting data is sent via a measurement computer to the HiSPARC data repository. Both stations have independent clocks in the master and slave units. These are synchronized using a GPS module in each station. Timing errors generated by this setup can be compensated because the cosmic ray flux from the zenith is at a maximum, leading in this case to equal arrival times for particles in both scintillators.

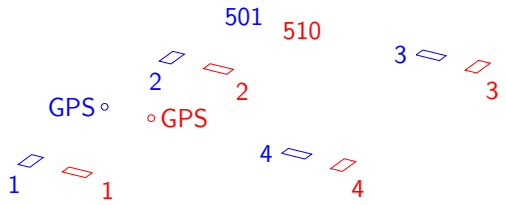

Fig. 3.1: *The map of stations* 501 *and* 510. *Station* 501 *is shown in blue,* 510 *is shown in red. A station consists of four scintillators* (1, 2, 3 *and* 4) *with areas of* $1000 \times 500\text{mm}^2$ *and a* GPS *antenna used for timing. The axes defined by detector pairs* 2 *and* 4 *are perpendicular to the axes defined by pairs* 1 *and* 3. *Distances* $d_{1,2}$, $d_{2,3}$, $d_{3,4}$, $d_{4,1}$ *and* $d_{2,4}$ *are all* 10m. *Distance* $d_{1,3}$ *is* 17.3m. *Distances between similar points in* 501 *and* 510 *are* 2m.

Scintillator pairs 2 and 4 (for both station 501 and 501) are regarded as single scintillator pairs. Scintillator pairs 1 and 3 (of both stations) are used to verify the theory of equal distributions. A data set over the periode from 5 October

2014 to 25 March 2015 is used. This set contains events where all scintillators have detected particles. Fig. 3.2 shows the measured distributions for the stations 501 and 510 for scintillators 2 and 4. Both distributions are compensated for systematic errors.

Using eq. 2.2 a curve fit is generated, leading to the exponent $a = 7 \pm 1$, the error along the N-axis is set on 5%.

To verify the theory, the data set is divided into subsets. Each subset is selected on a binned time difference for the scintillators 2 and 4. If the time difference is equal to the timing error, a slice through the zenith is selected. In fig. 3.3 the distributions for scintillator pairs 1 and 3 are shown for selected subsets with time differences 10ns apart. The measurements of each subset fit the plotted distribution with exponent $a = 7$ with an error along the N-axis of 5%.

Both plots in fig. 3.2 and fig. 3.3 show a discrepancy for larger angles. This partly can be explained by the size of the scintillators. These have an area of $1000 \times 500\text{mm}^2$. The distance between arriving particles is between 9.25m and 10.75m or 16.55m and 18.05m because paired scintillators are placed perpendicular towards each other. This results in an extra error of 7.5% for a scintillator distance of 10m and 4.5% (fig. 3.2) for a scintillator distance of 17.3m (fig. 3.3). Fig. 1.1 shows a simular discrepancy between measurements and the fitted curve.

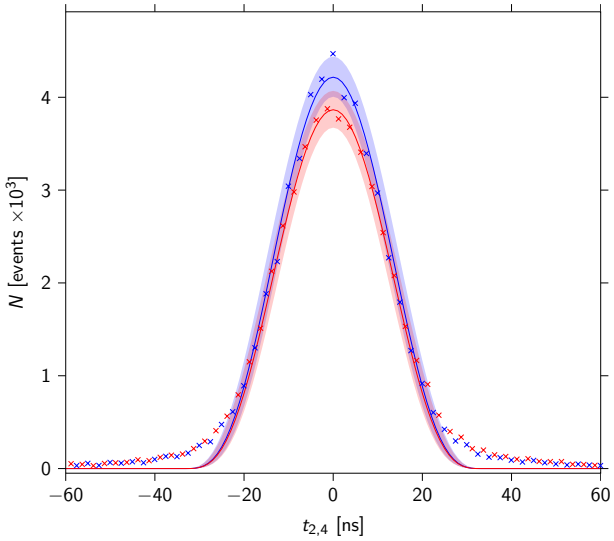

Fig. 3.2: *Distributions along the axis from scintillator 2 to 4 are shown. Data in the period from 5 October 2014 to 25 March 2015 using stations* 501 *(blue) and* 510 *(red) is binned in* 2.5 ns *wide bins and shown as crosses. The distributions for scintillator pairs 2 and 4 with distances of* 10m *are fitted. Shown distributions are calculated using* $a = 7 \pm 1$.

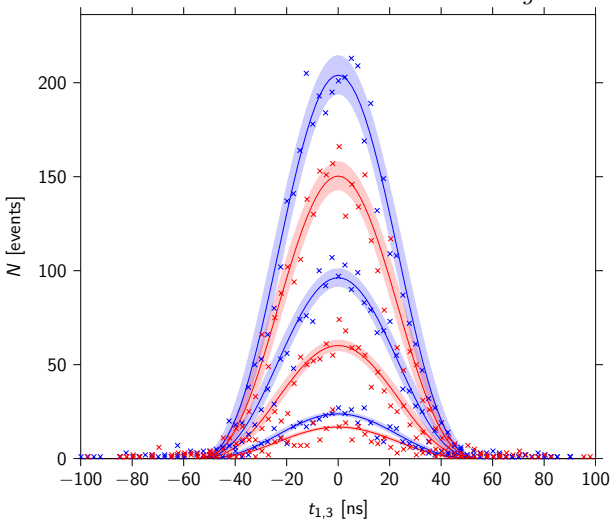

Fig. 3.3: *Distributions for the perpendicular pairs are shown. Measured particle showers are binned for time difference* $\triangle t_{2,4}$*, along the parallel axis from scintillator 2 to scintillator 4. The distribution along the perpendicular axis, from scintillator 1 to scintillator 3, is shown for three time differences (*$\triangle t_{2,4}$*)* 10[ns] *apart (*501 *is shown in blue and* 510 *in red). Shown distributions are calculated using* $a = 7 \pm 1$.

4 Reconstruction

A reconstrucion of the field of view of a scintillator pair starts with the measured arrival times $t_{m,1}$ and $t_{m,2}$ a time difference $t_{m,1\to2} = t_{m,2} - t_{m,1}$ is calculated. The setup as explained in sec. 3 generates constant delays for each scintillator leading to a timing error $t_{e,1\to2}$. The corrected time difference $t_{1,2}$ is calculated using the timing error $t_{e,1\to2}$: $t_{1,2} = t_{m,1\to2} - t_{e,1\to2}$. This corrected time difference of the arriving particles is used to reconstruct θ_{dt}.

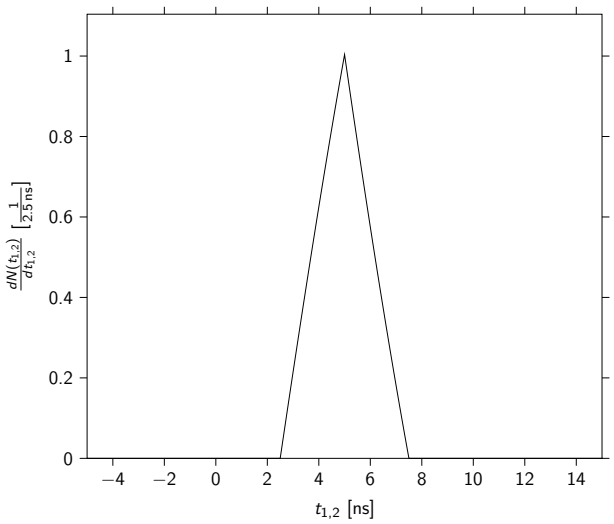

Fig. 4.1: *The probability distribution is at a maximum when a time difference is an exact measured binning time : ...,* −2.5ns, 0.0ns, 2.5ns, *... . There is a drop off when the difference moves to the bin edges. The sides of the triangle are slightly curved due to the particle distribution through the zenith.*

The angle θ_{dt} is calculated using eq. 1.2:

$$\theta_{dt} = \arcsin\left(\frac{c\,t_{1,2}}{d}\right) \tag{4.1}$$

The sample frequency of 400 MHz leads to a binwidth of 2.5 ns. The exact time difference is distributed over an interval of two measured bins. If the first time is close to the begin of the first bin and the second time is close to the end of the second bin there is a small chance of an extra bin time difference (and vice versa). This results in a triangular probability distribution $dn\,(t)\,/dt$.

Eq. 2.2 defines the number of particles in a binned slice with a time difference.

$$\frac{d^2N\,(t_{1,2}, w)}{dt_{1,2}dw} \propto \cos^a\left(\arcsin\left(\frac{c\,t_{1,2}}{d}\right)\right) \tag{4.2}$$

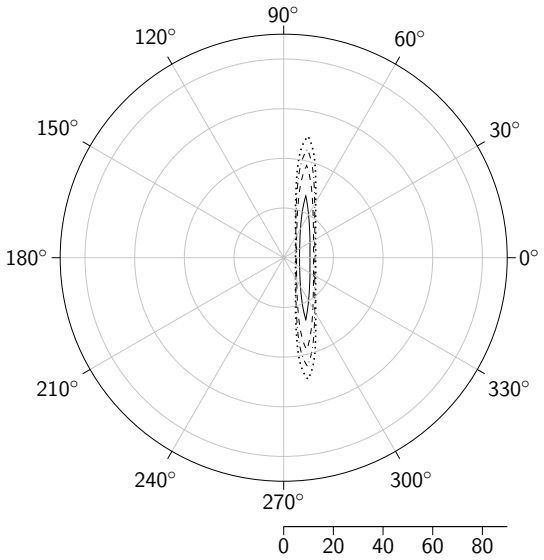

Fig. 4.2: Field of view for $t_{1,2} = 5\text{ns}$ *The field of view is shown in a* (θ, φ)*-plot for a detection with* $t_{1,2} = 5\text{ns}$ *and a scintillator distance of* 10m, θ *is plotted along the radius. The curves correspond with probabilities of* 5% *(dotted),* 10% *(dash dotted),* 20% *(dashed) and* 50% *(solid). The scintillators are locared on the axis* 0^o / 180^o*, as a result the angle* θ_{dt} *is along the* 0^o / 180^o *axis and the angle* $\theta_\perp$ *is along the* 90^o / 270^o *axis.*

Using the triangular distribution $dn\left(t\right)/dt$ the number of particles is calculated for a given time.

$$\frac{d^2N\left(t,w\right)}{dtdw} = \frac{dN\left(t\right)}{dt} \times \frac{d^2N\left(t_{1,2},w\right)}{dt_{1,2}dw} \tag{4.3}$$

This resulting distribution of time differences[3] is shown in fig. 4.1 for a corrected time difference of $t_{1,2} = 5.0\,\text{ns}$. The distribution of time differences follows a triangle, slightly deformed due to the curvature of the particle distribution as a function of the time difference.

The angle $\theta_\perp$ now can be calculated for a given chance. Fig. 4.2 shows these curves for several chances defining the field of view for a time difference in detections.

[3] Normalised for a single particle.

5 Conclusion

A single scintillator has a wide field of view, a scintillator pair has a an increased accuracy along the axis through both scintillators. Mathematical analysis shows that all distributions of particles in planes perpendicular to the Earth's surface are isomorphous. The time difference defines a cone of arrival for particles in an EAS. Distributions in this cone and perpendicular on this cone are simular. This is verified using four scintillators placed on perpendicular axes in the HiSPARC stations 501 and 510. The size of the scintillators and the thickness of the EAS front are not taken into account. Discrepancies between theory and measurements are however small.

Using this theory the field of view of a scintillator pair can be reconstructed using the time difference. Comparing the theoretical field of view with the simulation of a detector pair both show an elongated band across the sky.

The author wishes to thank J.J.M. Steijger for many critical discussions.

References

[1] A. de Laat et al. EAS direction reconstruction with HiSPARC. Poster presented at ISVHECRI-2014.

[2] K. Greisen. The extensive air showers in J.G. Wilson (ed.). *Progr.Cosmic.Ray.Phys.*, 3, 1956.